ISSN 0031-918X, Physics of Metals and Metallography, 2020, Vol. 121, No. 1, pp. 53–64. © Pleiades Publishing, Ltd., 2020.
Russian Text © The Author(s), 2020, published in Fizika Metallov i Metallovedenie, 2020, Vol. 121, No. 1, pp. 60–71.

STRUCTURE, PHASE TRANSFORMATIONS, AND DIFFUSION

Atom Probe Tomography of the VV751P Nickel-Based Superalloy

S. V. Rogozhkin[a, b, *, **], L. B. Ber[c], A. A. Nikitin[a, b], A. A. Khomich[a], O. A. Raznitsyn[a], A. A. Lukyanchuk[a], A. S. Shutov[a], M. M. Karashaev[c], and A. G. Zaluzhny[a, b]

[a] *Alikhanov Institute of Theoretical and Experimental Physics, Kurchatov Institute National Research Center, Moscow, 117218 Russia*

[b] *National Research Nuclear University MIFI, Moscow, 115409 Russia*

[c] *JSC All-Russia Institute of Light Alloys (VILS), Moscow, 121596 Russia*

**e-mail: Sergey.Rogozhkin@itep.ru*

***e-mail: SVRogozhkin@mephi.ru*

Received June 25, 2019; revised June 25, 2019; accepted July 26, 2019

Abstract—This work presents the results of the study of three different blanks used for the production of disks for gas-turbine engines made of a granular Ni-based superalloy. The blanks differed in the heat treatments performed and in the complexes of mechanical characteristics. The scanning electron microscopy of the studied materials showed that the size of the γ-matrix grains was 30–50 micrometers. In addition, particles of the γ and γ′ phases with a size from 10 to 70 nm were revealed in the volumes of all blanks. The morphology of these particles has been studied. Within the particles of the γ′ phase, homogeneously distributed equiaxed clusters of atoms of γ-forming elements were revealed with a size of 1–4 nm and flattened clusters of the same size and the same chemical composition aligned into chains. In the particles of both phases and in the transition layers between them, concentrations of the alloying components and impurities have been determined. In the studied volumes of the three different blanks of the disks, the volume fractions of the γ′ phase were found to be 68 ± 1, 61 ± 2, and 62 ± 4%.

Keywords: Ni-based superalloy, atom-probe tomography, nanostructure

DOI: 10.1134/S0031918X20010123

INTRODUCTION

Nickel-based superalloys (NBSAs) used for the production of gas-turbine engines (GTEs) are divided into alloys for gas-turbine blades, disks, and alloys for other parts of the hot tracts of GTEs. The blades and disks refer to parts with a highly responsible role. They operate under extreme and fundamentally different conditions [1–4]. The main requirement of the NBSAs used for blade production is a high resistance to fatigue at temperatures of 950–1100°C and stresses of 150–250 MPa [2, 4]. To ensure the necessary reserve of serviceability, the new generations of NBSAs for disks must meet hard and hardly compatible requirements: at temperatures ranging from room temperature to ~550°C, they should have an ultimate strength $\sigma_u \geq 1500$ MPa, a yield stress $\sigma_{0.2} \geq 1150$ MPa, a relative elongation $\delta \geq 12$ per cent, and a *KCU* (impact toughness of a sample with a U-shaped notch) ≥ 24 J/cm^2. At 650°C and $\sigma = 1078$ MPa, the lifetime upon tests for long-term strength of smooth samples and of notched samples should be ≥ 100 h [3]. The number of cycles upon the tests for the low-cycle fatigue (LCF) ($T = 650$°C, $\sigma = 1098$ MPa) should be ≥20000.

To understand the laws of the influence of alloying and heat treatment on the mechanical characteristics and operational properties of the NBSAs, it is important to know the structural and phase states of the alloys and the chemical composition of their phase components [5], first of all, of the γ solid solution highly alloyed with transition metals and of the particles of the γ′ phase distributed in this volume (with a volume fraction of ≥ 50%), as well as of particles of carbides, borides, and carboborides. These data help one to choose the optimal chemical composition of the alloy and the temperature and time conditions of the stages of the manufacturing process, which determine the complex of properties and the service reserve of parts under operation conditions [6, 7]. To find the details of the structural-phase state of the NBSAs on the atomic level, studies involving the application of atom probe tomography (APT) have been widely initiated [8, 9].

The purpose of this work is the APT investigation of the structure of commercial large scale blanks of

Table 1. Chemical composition of the VV751P alloy

	Co	Cr	V	C	W	Ni	Mo	Ti	Nb	Al	Hf	B
wt %	15.3	11	0.6	0.055	3.0	55.49	4.5	2.8	3.3	3.9	0.05	0.002
at %	14.95	12.19	0.67	0.26	0.94	54.48	2.7	3.38	2.04	8.32	0.016	0.008

disks produced from the new granular high-strength NBSA VV751P developed at the JSC "VILS" (All-Russia Institute of Light Alloys). The VV751P alloy is the base material for the production of disks for gas-turbine engines ("PD-14") for domestic passenger liners MS-21 and military transport aircrafts IL-276. The morphology and chemical composition of nanosized particles of the γ and γ' phases have been studied, as well as the interphase boundaries between them, and the peculiarities of the spatial location of particles of the γ and γ' phases.

EXPERIMENTAL

The chemical composition of the structural components of the material was studied using the APPLE-3D atom probe tomograph with the femtosecond laser-assisted evaporation designed at the Institute of Theoretical and Experimental Physics, "Kurchatov Institute" National Research Center [10, 11]. The study was carried out using a detector based on the DLD80 delay lines with a detection efficiency of ~90%. The 3D reconstruction of the location of atoms in the sample was carried out using the "KVANTM-3D" software [12].

The data were obtained at a constant voltage of 2–9 kV at the sample, laser-pulse duration of 300 fs, laser frequency of ~11 mW, the harmonic of 515 nm, the temperature of the sample equal to 50 K, and the vacuum in the process of the investigation on the level of $(5–7) \times 10^{-10}$ Torr. The optimization of the conditions of the data acquisition was performed as in [13].

For the APT studies, samples in the form of needles with the radius of the rounding of the tip equal to several tens of nanometers were used. The samples were prepared using electroerosion cutting and subsequent electrochemical thinning of the blank up to obtaining the required shape of the tip. The shape of the tip was controlled with the help of a JEOL 1200 EX electron microscope.

The processing of the experimental APT data included the identification of the spectra obtained in the APPLE-3D setup by the time-of-flight mass spectroscopy and the analysis of 3D distributions of chemical elements in the volumes investigated. For coarse inclusions of secondary phases, cross-sectional profiles were plotted and an analysis of linear concentrations was performed, and volumes from inside these objects were cut out to obtain concentrations of elements in these phases. For the description of the structure elements with the sizes less than 10 nm, the method of the maximum separation was used. In this work, the procedure of the search for the most reliable parameters of this method for different nanoscaled features was carried out separately.

To analyze the microstructure of the samples on a larger scale, the studies by the scanning electron microscopy (SEM) using the KYKY-2800B microscope were carried out.

MATERIALS

The material of serial large-scale blanks for the production of disks with the conditional numbers 1, 2 and 3 of the alloy VV751P melted using ingots of approximately the same chemical composition (presented in Table 1) was examined. The content of impurities and alloying additives such as Ce, La, and Sc was lower than the sensitivity of the techniques of spectral analysis used in the JSC "VILS."

The blanks 1–3 were obtained according to the following scheme: (1) the vacuum-induction melting of a cylindrical ingot for further dispersion into granules; (2) the plasma-arc melting and centrifugal sputtering of a rapidly rotating cast ingot (Plasma Rotating Electrode Process, PREP) with the preparation of granules 50–100 μm in size; (3) hot isostatic pressing (HIP) of the granules in a steel capsule; (4) heat treatment of the ingots after HIP, including heat treatment for solid solution in a vacuum, rapid cooling by gaseous helium (quenching) at a pressure of more than 2 atm, and two- or three-stage aging.

Blanks 1 and 2 were prepared in a MODULTERM vacuum furnace with the temperature interval for the solid-solution treatment (SST) of 1200–1215°C; blank 3, in a MONOTERM vacuum furnace with the temperature of the SST equal to 1210°C. The holding upon SST for all the blanks was 4–8 hours.

For blanks 1 and 3, a three-step aging was used; for blank 2, a two-step aging. The principles for the choosing of the temperatures and times of the quenching-cooling route are described in [15]. The temperature–time cooling routes and aging regimes used are the KNOW-HOW of the JSC "VILS."

The mechanical properties of the samples made from the disk blanks 1–3 at room temperature and the characteristics of long-term strength and LCF at 650°C are presented in Table 2.

Table 2. Mechanical properties of samples made from blanks 1, 2 and 3 used for the production of disks (at 20 and 650°C)

Blank no.	Mechanical properties at 20°C					Long-term strength, h (T = 650°C, σ = 1078 MPa)		LCF, number of cycles (T = 650°C, σ = 1098 MPa)
	σ_u, MPa	$\sigma_{0.2}$, MPa	δ, %	ψ, %	*KCU*, J/cm^2	τ_{sm}	τ_n	
1	1570	1160	18.5	20.5	24	177	383	25930
	1560	1190	20.5	15.0	20	183	383	–
2	1570	1190	19.0	18.5	29	104	377	25720
	1570	1180	15.0	20.5	30	149	14	–
3	1550	1130	17.0	19.5	28	137	146	31090
	1540	1140	17.0	18.0	26	–	–	–

τ_{sm} is the time to failure of a smooth sample; τ_n is the time to failure a notched sample.

It can be seen that σ_u and $\sigma_{0.2}$ of the samples cut out from blanks 1 and 2 are higher than the σ_u and $\sigma_{0.2}$ values of the samples cut out of blank 3. The higher values of these characteristics correspond to the smaller size of the γ′-phase particles in the blanks, which is due to the higher rate of cooling of blanks 1 and 2 upon quenching.

STUDIES USING THE SEM METHOD

Figure 1 presents the results of the investigation of the microstructure of the disk blanks 1–3 by SEM used in secondary electron mode. The size of the γ-matrix grains is 30–50 μm. Against the background of a relatively bright γ phase (matrix, with an fcc lattice), darker cuboidal submicroscopic particles of the γ′ phase can be seen in the bulk of grains with the ordered $L1_2$ crystal lattice formed in the process of the decomposition of the γ solid solution upon quenching cooling and subsequent aging. These particles have sizes of 0.15–0.25 μm. Because of the proximity of the lattice parameters a_γ and $a_{\gamma'}$, the particles of the γ and γ′ phases are coherent. The particles of the γ′ phase formed and grow during the decomposition of supersaturated γ solid solution; their volume fraction increases. When the size of a cuboid exceeds ~0.5 μm, the cuboid shape of the particle becomes unstable because of the increase of internal coherent elastic stresses proportional to $(a_{\gamma'} - a_\gamma)^2$. Because of the small interphase surface energy, the separation of one cuboid particle into an octet of eight particles becomes energetically profitable (Figs. 1b and 1c). At the grain boundaries, the γ′-phase particles have a platelet shape and a size of 0.3–0.8 μm. The brightest particles in Figs. 1a and 1b are the carbides and carboborides of the type M(B, C) with a size of 0.3–1.0 μm, where M is Ti, Nb, or Hf.

RESULTS OF THE APT STUDY

Sample Cut Out from Blank 1

Figure 2 shows the maps of the distribution of atoms in the studied volume of the sample of blank 1. The quantitative data about the content of elements in γ-phase particles ($C_{i\gamma}$) and in γ′-phase particles ($C_{i\gamma'}$) are given in Table 3.

It has been revealed that the values of $C_{i\gamma'}$ for the Ni, Al, Ti, and Nb atoms are significantly greater (by 2–30 times) than the corresponding values of $C_{i\gamma}$, and for

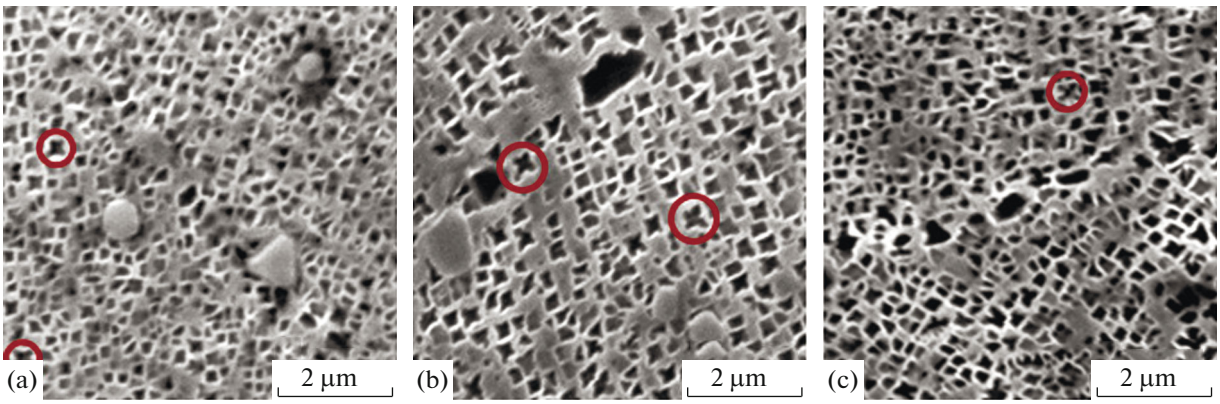

Fig. 1. SEM images of the microstructure of samples made of the blanks (a) 1, (b) 2, and (c) 3. In the circles, octets can be seen.

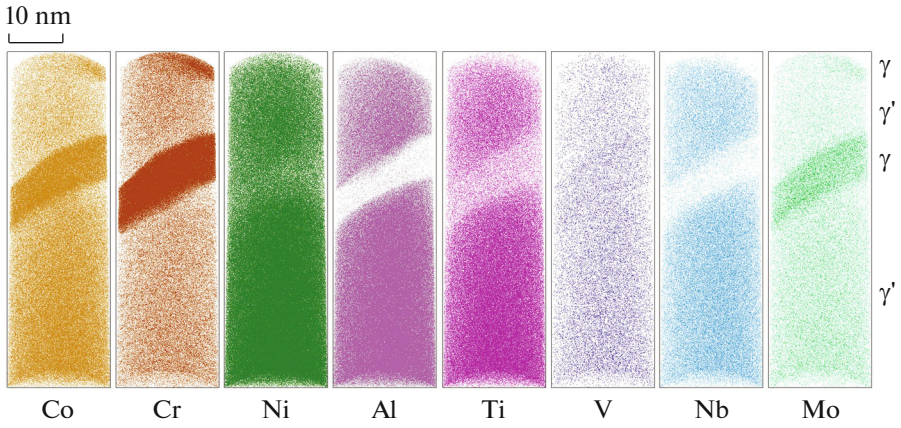

Fig. 2. Atomic maps of the distribution of chemical elements in the studied volume of the blank 1. The number of registered atoms is ~4×10^6.

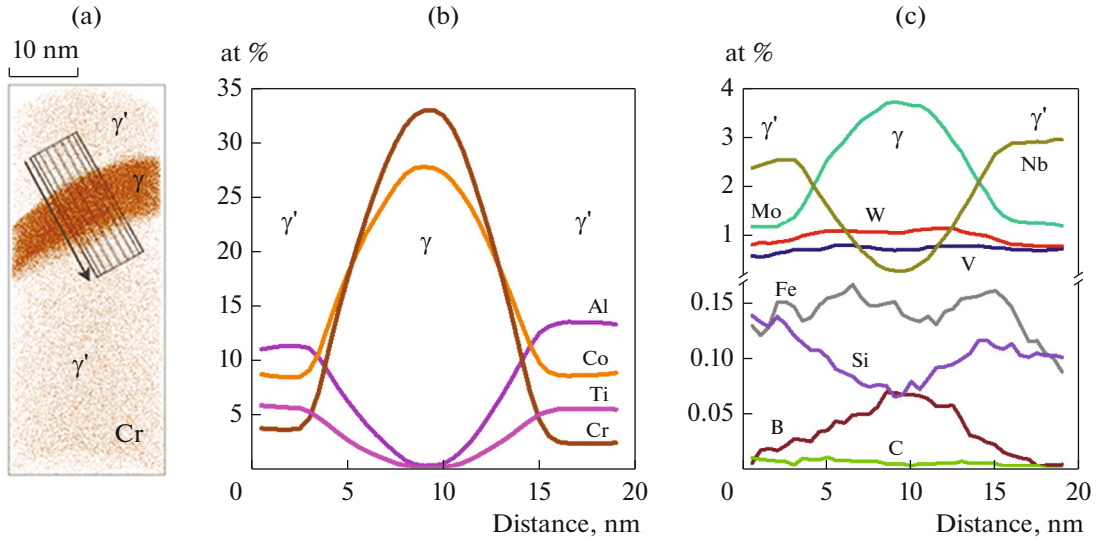

Fig. 3. (a) Procedure of cutting out of a cylindrical region used for the construction of linear concentration profiles. In (a), the distribution of Cr atoms is shown; in (b) and (c), concentration profiles along the line crossing the γ-phase particle shown in Fig. 1a. Blank 1.

Co, Cr, and Mo atoms, the $C_{i\gamma}$ values are substantially greater (by 3–8 times) than the corresponding values of $C_{i\gamma'}$. The content of W, Fe, and Si in the γ phase is 1.2–1.5 times greater than in the γ' phase, and that of atoms B in the particles of the γ' phase is 1.3 times larger than in the γ-phase particles.

To analyze the chemical composition of particles of the γ and γ' phases and the thickness of the transition layer between them, concentration profiles were plotted along the line crossing the γ-phase particle. Figure 3 illustrates the procedure of cutting out samples from the examined cylindrical region for the plotting of concentration profiles and the concentration profiles themselves.

The values of the concentrations $C_{i\gamma}$ (from Table 3) were used to estimate the volume fraction of the γ' phase in the studied volume by the lever rule: $f_{\gamma'} = (C_n - C_\gamma)/(C_\gamma - C_{\gamma'})$, where C_n is the average content of the i-th element in the material.

Figure 4a shows the dependence of the difference $(C_n - C_\gamma)$ on the difference $(C_\gamma - C_{\gamma'})$. The value $f_{\gamma'}$ of the volume fraction of the γ' phase in the studied volume of blank 1 calculated based on the slope of the straight line (obtained by the method of least squares of deviations) is 68 ± 1%.

Sample of Blank 2

Figure 5 shows the distribution of atoms in the studied volume of blank 2. The contents of the various elements $C_{i\gamma}$ and $C_{i\gamma'}$ for the sample cut out from blank 2

Table 3. Concentrations of chemical element (at %) in the particles of the γ phase (C_γ) and of the γ′ phase ($C_{\gamma'}$) in the investigated volumes of the blanks 1–3 (APT analysis)

No.	Phase	Co	Cr	V	Fe	C	Si	W	Ni	Mo	Ti	Nb	Al	B
1	γ	27.9 ± 0.1	32.8 ± 0.1	0.71 ± 0.02	0.19 ± 0.01	0.003 ± 0.001	0.109 ± 0.008	1.05 ± 0.02	33.4 ± 0.1	3.07 ± 0.04	0.12 ± 0.01	0.26 ± 0.01	0.34 ± 0.01	0.012 ± 0.002
	γ′	8.15 ì± 0.05	4.23 ± 0.04	0.68 ± 0.01	0.15 ± 0.01	0.014 ± 0.003	0.079 ± 0.005	0.73 ± 0.02	65.13 ± 0.08	0.97 ± 0.02	5.75 ± 0.04	2.82 ± 0.03	11.29 ± 0.05	0.092 ± 0.007
2	γ′	9.6 ± 0.1	1.8 ± 0.1	0.59 ± 0.03	0.06 ± 0.01	–	–	0.46 ± 0.03	66.1 ± 0.2	1.03 ± 0.04	5.83±0.09	1.99 ± 0.06	12.5 ± 0.1	0.02 ± 0.01
	*γ′	10.3 ± 0.1	5.2 ± 0.1	1.01 ± 0.04	0.17 ± 0.02	–	0.09 ± 0.02	0.87 ± 0.04	62.4 ± 0.2	1.76 ± 0.07	3.32 ± 0.08	2.06 ± 0.06	12.7 ± 0.2	0.06 ± 0.01
	γ	24.7 ± 0.1	30.6 ± 0.1	0.81 ± 0.02	0.19 ± 0.01	0.007 ± 0.006	0.04 ± 0.01	0.96 ± 0.03	37.8 ± 0.1	3.77 ± 0.05	0.09 ± 0.01	0.35 ± 0.01	0.5 ± 0.1	0.07 ± 0.01
	*γ	19.3 ± 0.3	15.6 ± 0.3	0.42 ± 0.05	0.08 ± 0.02	–	0.04 ± 0.02	0.38 ± 0.04	49.9 ± 0.4	1.04 ± 0.07	4.4 ± 0.2	1.38 ± 0.08	7.5 ± 0.2	–
3	γ′	12.85 ± 0.02	1.78 ± 0.01	1.17 ± 0.01	0.32 ± 0.01	0.094 ± 0.001	–	1.17 ± 0.01	63.6 ± 0.1	1.63 ± 0.01	4.89 ± 0.01	0.49 ± 0.01	11.97 ± 0.02	0.010 ± 0.001
	*γ′	22.46 ± 0.03	26.47 ± 0.04	0.88 ± 0.01	1.03 ± 0.01	0.042 ± 0.002	–	1.30 ± 0.01	41.4 ± 0.1	3.01 ± 0.01	1.04 ± 0.01	0.30 ± 0.01	2.02 ± 0.01	0.020 ± 0.001
	γ	24.11 ± 0.02	29.33 ± 0.02	0.95 ± 0.01	0.58 ± 0.01	0.120 ± 0.002	0.088 ± 0.002	1.11 ± 0.01	38.5 ± 0.1	3.83 ± 0.01	0.17 ± 0.01	0.23 ± 0.01	0.93 ± 0.01	0.026 ± 0.001

*γ′—pre-precipitate of the γ′ phase; *γ—pre-precipitate of the γ-phase.

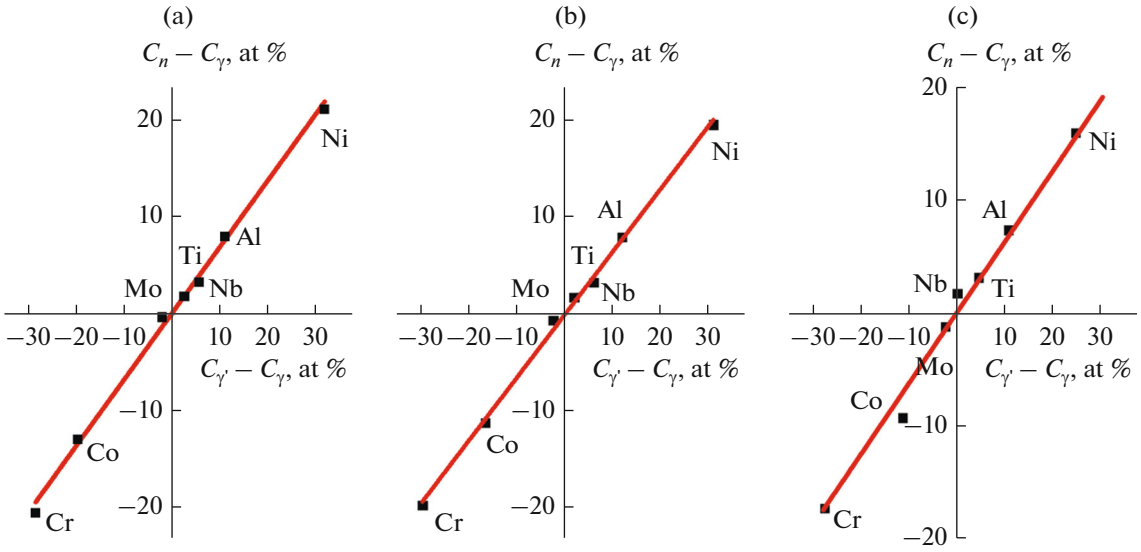

Fig. 4. Dependences of the differences of the average concentration of the element and its concentration in the γ phase ($C_n - C_\gamma$) on the difference of the atomic concentrations of the elements in the γ and γ′ phases ($C_\gamma - C_{\gamma'}$) in the samples made from the blanks (a) 1, (b) 2, and (c) 3.

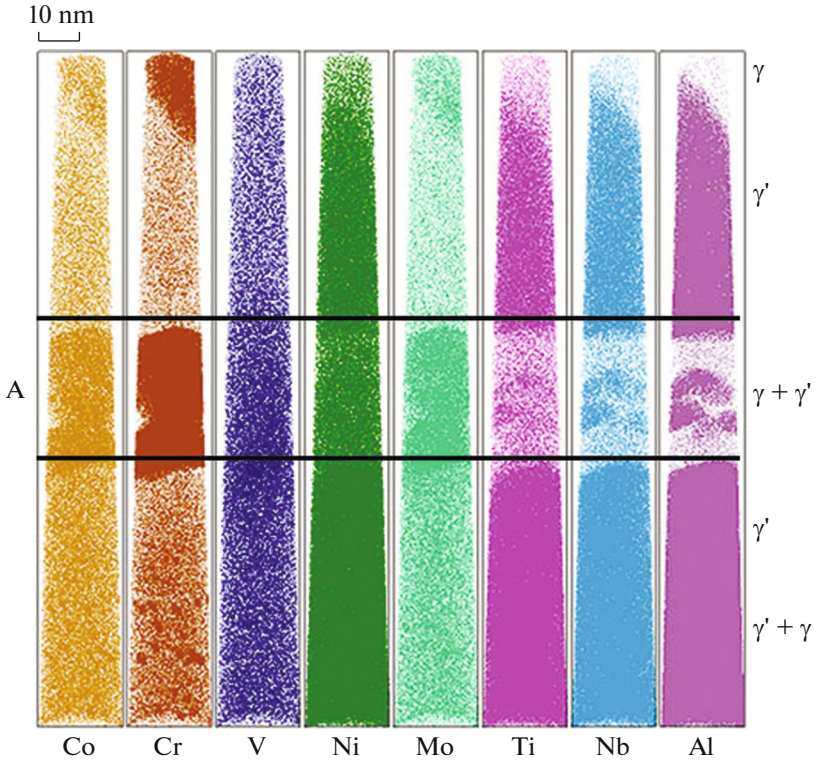

Fig. 5. Atomic maps of the distribution of chemical elements in the invesigated volume of blank 2. The number of registered atoms is ~2×10^7.

are also collected in Table 3. A small γ-phase particle is located at the top part of the studied volume (Fig. 5); below it, there is a particle of the γ′ phase; and still lower, there is a γ-phase particle in which there are four to five particles of the γ′ phase.

For a more detailed analysis of this volume, a region A is separated (by horizontal straight lines) in Fig. 5. Within this region, we can see a particle of the γ phase with a vertical size of ~35 nm, inside which particles of the γ′ phase 11 ± 4 nm in size (pre-precip-

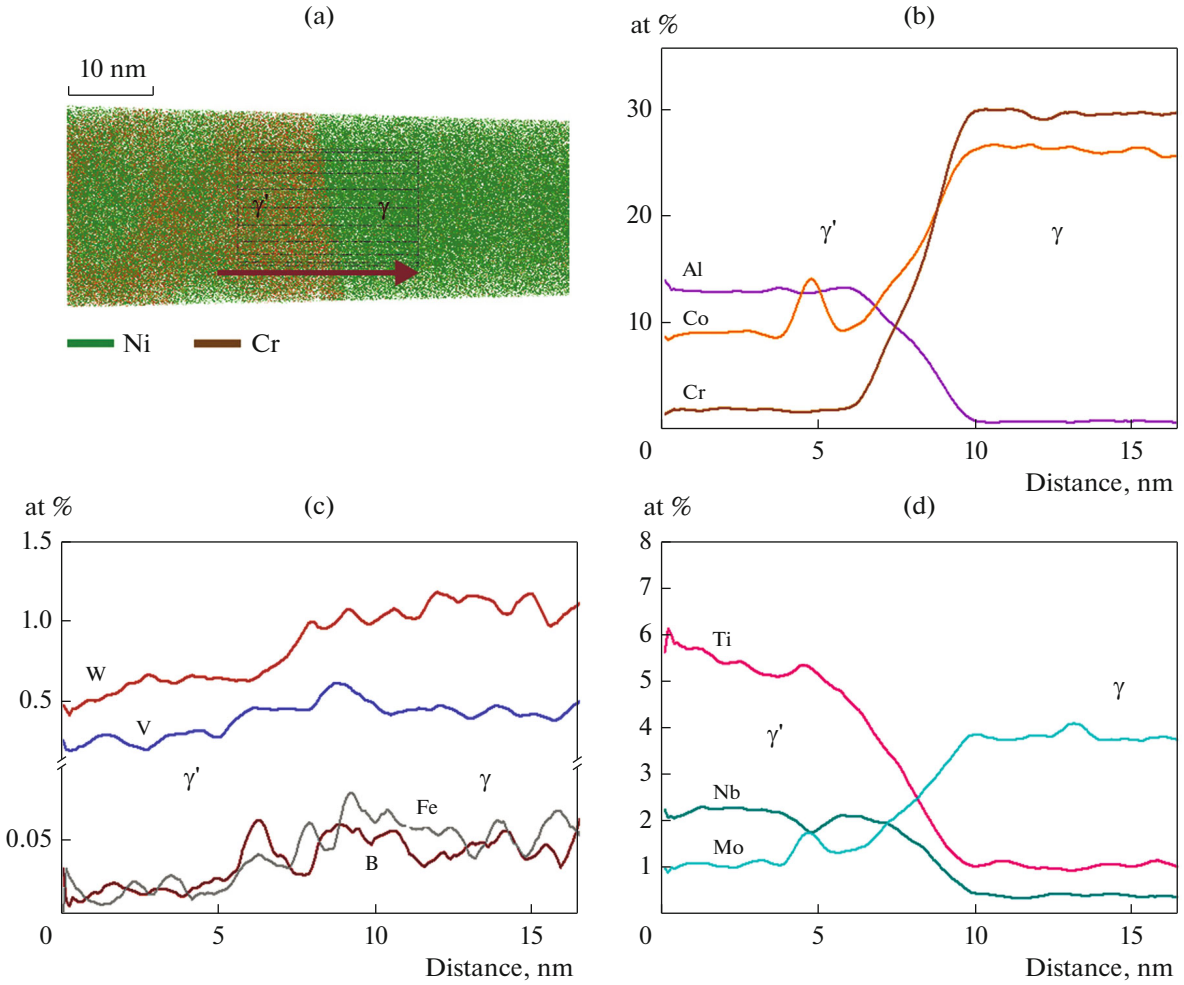

Fig. 6. Linear concentrations along the line that crosses one of the detected γ-phase particles in the studied volume of blank 2 (APT analysis).

itates of the γ′ phase) are located. The number density of these particles is ~10^{23} m^{-3}. At the bottom of the volume investigated, a coarse particle of the γ′ phase is located, with homogeneously distributed equiaxed clusters (1–4 nm in size) of Cr and Co atoms (pre-precipitates of the γ phase).

Figure 6 shows the concentration profiles of various elements inside the fragment A that contains a transition layer between the particles of the γ′ phase and γ phase. The direction of the normal to this particle of the γ phase is indicated by an arrow.

Figure 7a shows a map of the distribution of Al and Co atoms in the volume shown in Fig. 5; in Fig. 7b, an enhanced image of the distribution of atoms of Al, Ti, and Nb in the region outlined in Fig. 7a is given. It can be seen that the atoms of these elements are present in both the γ-phase particles and in the γ′-phase particles, but their concentration is significantly higher in the γ′-phase particles.

In Fig. 8a one of the particles of the γ′ phase ~6 × 10 nm in size located in the region A of Fig. 5 is shown,

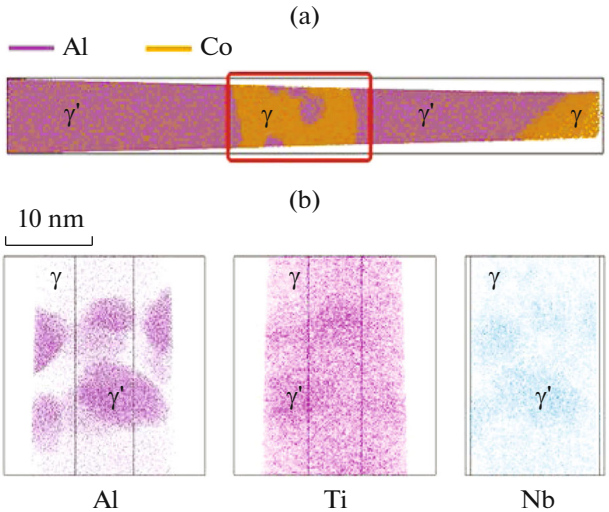

Fig. 7. (a) Atom maps of the distribution of Al and Co atoms in the studied volume of blank 2; and (b) atom maps of the distribution of Al, Ti, and Nb atoms in the rectangle shown in Fig. 7a by red lines.

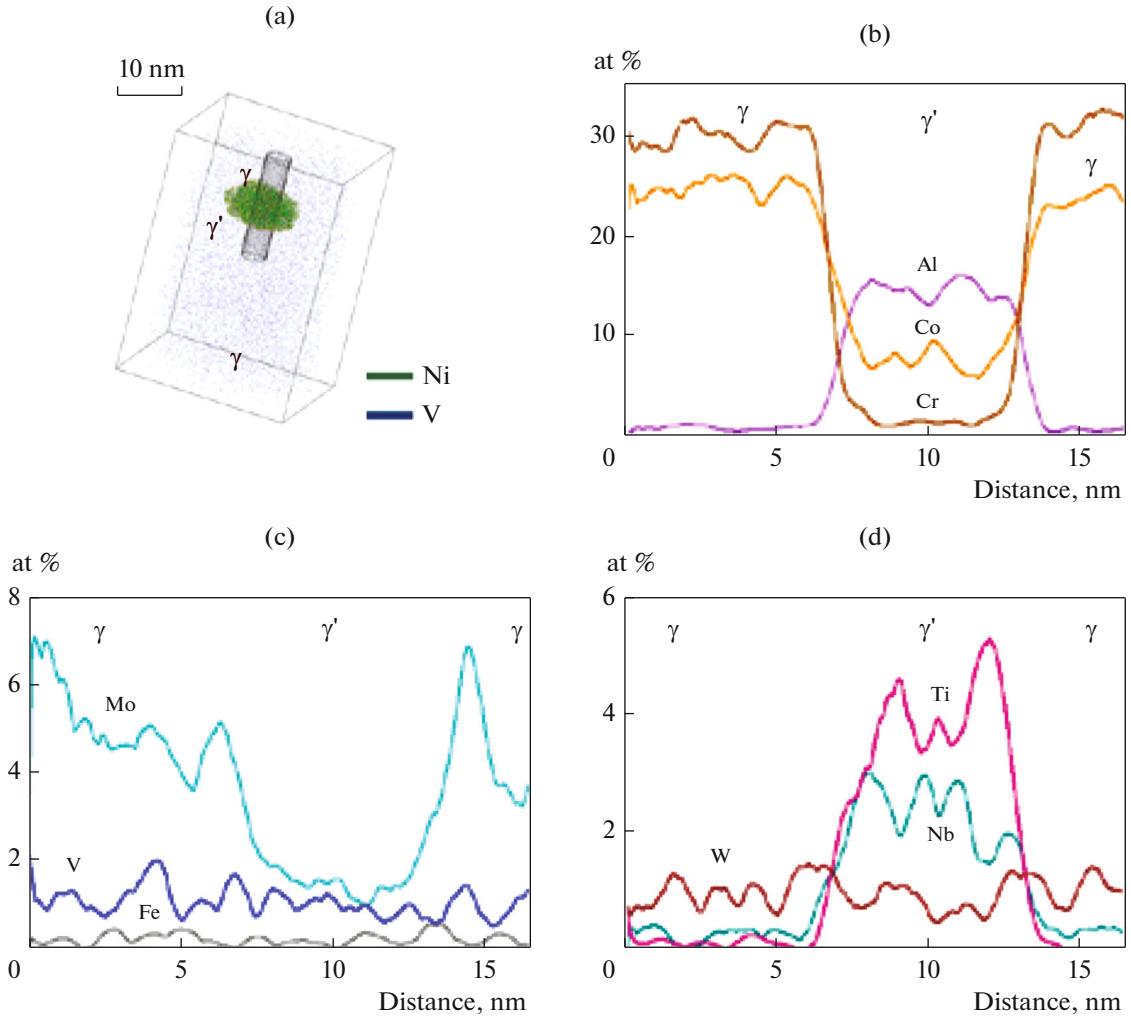

Fig. 8. Concentration profiles of the distribution of elements along the line crossing one of the particles of the γ′ phase in the studied volume of blank 2.

and concentration profiles of the distribution of atoms along the line intersecting this particle are also shown. In the analyzed particle of the γ′ phase, the concentrations of Al, Ti, and Nb are significantly higher, and those of Mo, Co, and Cr are significantly smaller than in the γ phase. The concentrations of W, V, and Fe in this γ′-phase particle and in the surrounding γ matrix are approximately the same.

On the maps of distribution of the Co and Cr atoms inside a large (more than 30 nm along the vertical) γ′-phase particle at the bottom part of Fig. 5, homogeneously distributed clusters (1.5–2.0 nm in size) of Co and Cr atoms can be seen.

In the other part of blank 2 (Fig. 9), chains of ultradisperse flattened regions of Co, Cr, and Mo atoms depleted of Al and Ni can be seen. The average size of these regions is ~2 ± 1 nm. Concentration profiles perpendicular to these chains have been plotted (Fig. 10). The concentrations of Ti atoms, which are usually much higher in the γ′ phase than in the γ phase, are close in these regions and in the surrounding γ′ phase. The contents of the V, Fe, Nb, and W atoms in these regions and in the γ′ phase also are almost the same.

For the studied volume of blank 2, the diagram of the dependence of $(C_n - C_\gamma)$ on $(C_\gamma - C_\gamma)$ in Fig. 4b has been plotted. The value of the volume fraction of the γ′ phase in this volume obtained from the slope of the straight lines is ~61 ± 2%.

Sample Made from Blank 3

The maps of the distribution of atoms of various elements in the examined volume of the sample made from blank 3 are presented in Fig. 11, and the data on the content of the elements are presented in Table 3.

In regions *1* and *2*, a γ-phase particle with a vertical size of more than 130 nm can be seen. In region *2*, inside this particle, a flattened particle of the γ′ phase with a size of ~7 × 13 nm is observed. In region *3*, to the right

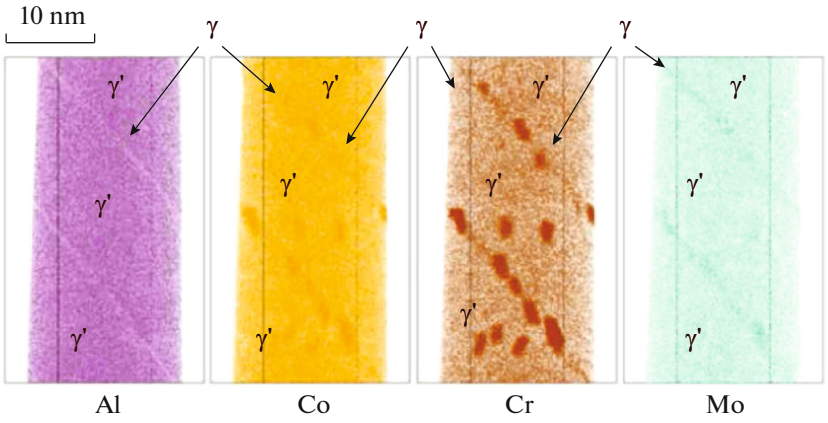

Fig. 9. Atomic maps of distribution of Al, Co, Cr, and Mo in a fragment of the studied sample of the blank 2.

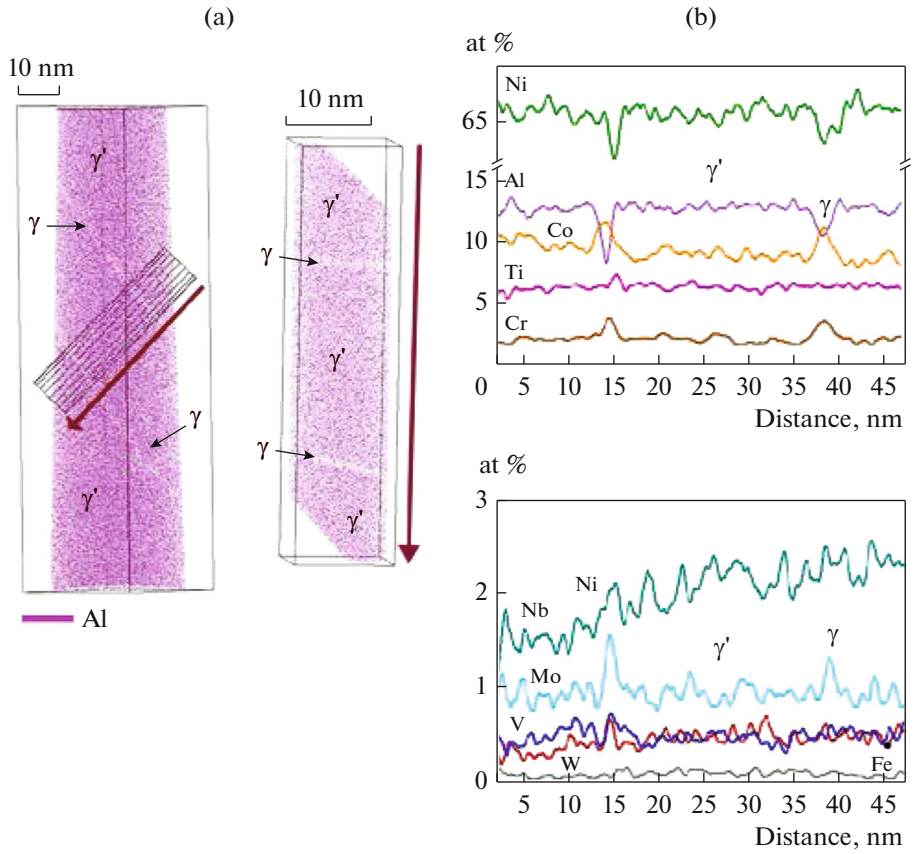

Fig. 10. (a) Maps of the distribution of Al atoms in the studied volume of the blank 2; (b) profiles of linear concentrations of chemical elements along the line that crosses chains of γ-phase pileups (see volume outlined in Fig. 10a).

and to the left of the γ'-phase particle with a size of >70 nm, there are two regions of the γ phase and one more region of the γ phase below this particle. The concentration profiles obtained along the line that crosses the γ'-phase particle in region *2* are shown in Fig. 12.

Figure 13 shows the concentration profiles of the transition layer between the γ'-phase particle and the region of the γ phase located at the boundary between the regions *2* and *3*. The particle of the γ' phase is enriched in Al, Ti, Nb, and V. In the γ phase the content of Co, Cr, Mo, and Fe is higher (see Table 3). The

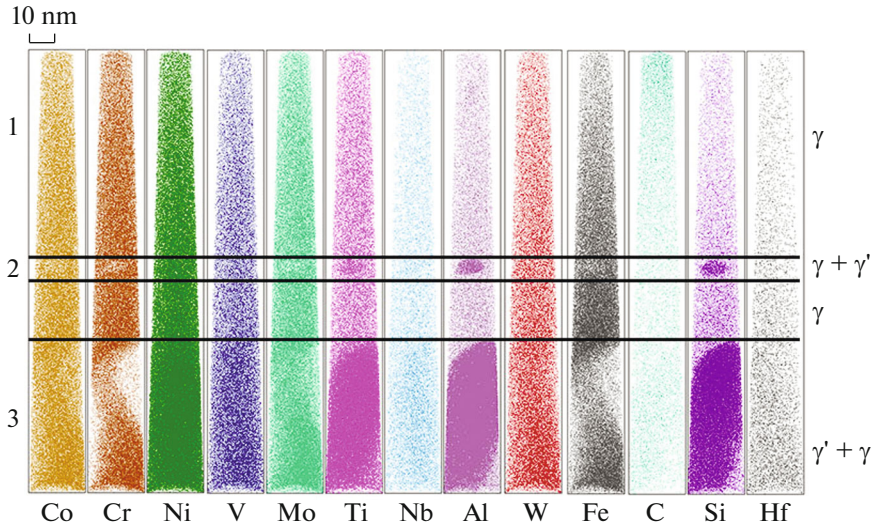

Fig. 11. Atomic maps of the distribution of chemical elements in the studied volume of the blank 3. The separated regions: (1) γ phase; (2) γ'-phase particle in the γ phase; and (3) particles of the γ and γ' phases.

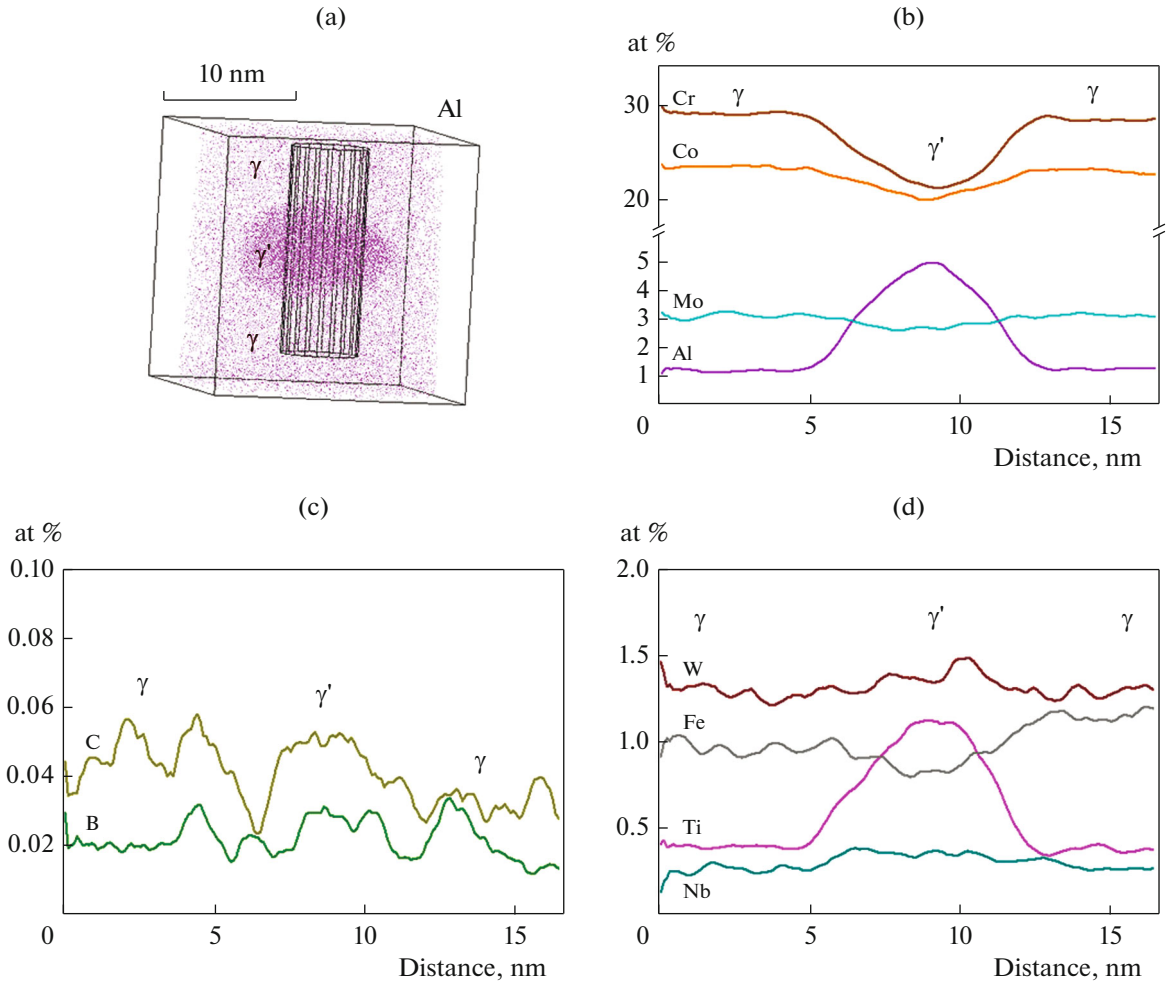

Fig. 12. Concentration profiles of the distribution of chemical elements along the line crossing the γ'-phase particle in region 2 (Fig. 11). Blank 3.

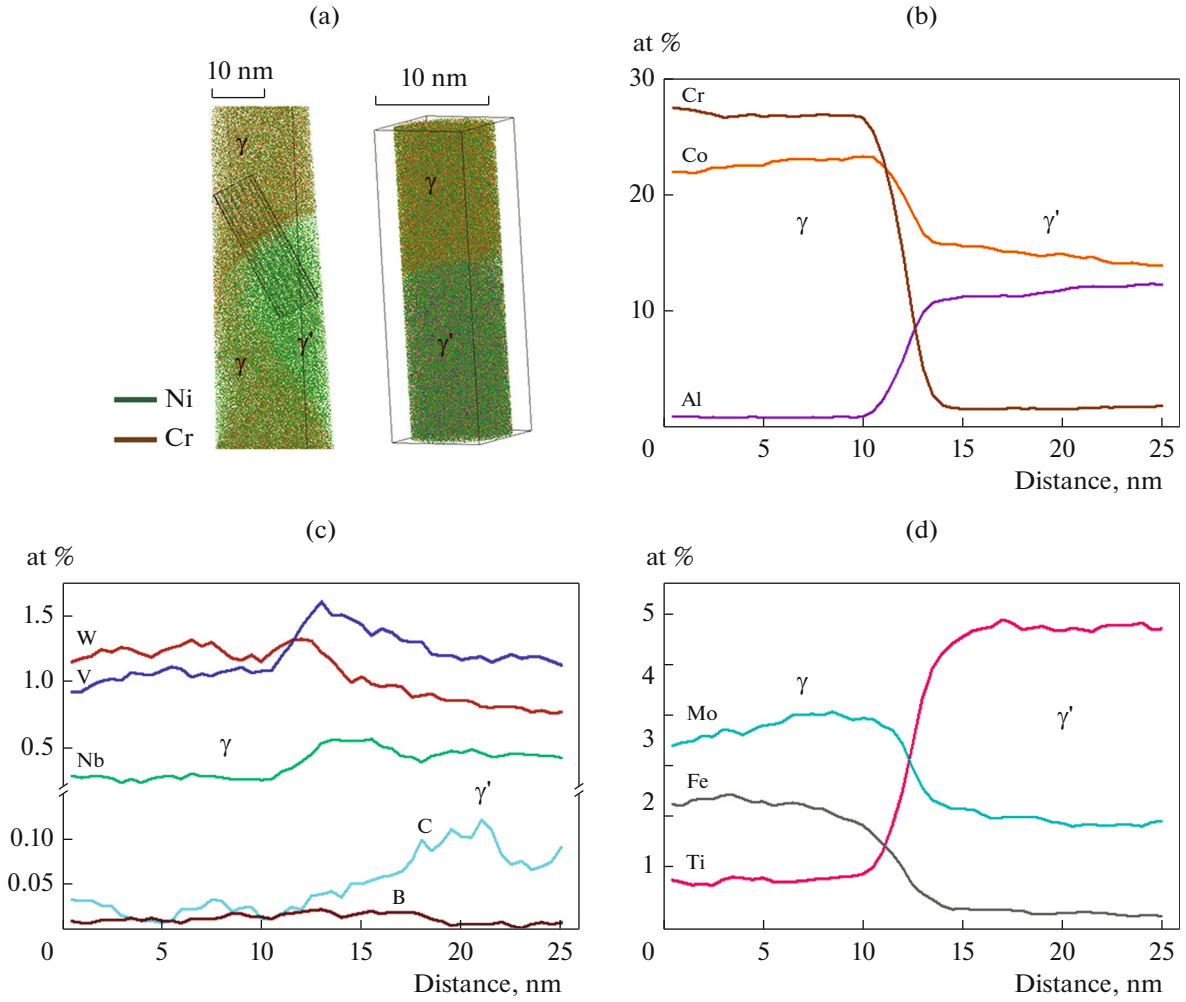

Fig. 13. Concentration profiles of the distribution of elements along the line perpendicular to the boundary between the γ-phase particle located in the regions 1 and 2 and γ′-phase particle in the region 3 (Fig. 12). Blank 3.

W content in both phases is approximately the same. The contents of B and C in the γ and γ′ phases in the sample of blank 3 have no pronounced trends.

The analysis of the dependence presented in Fig. 4c shows that the volume fraction of the γ′ phase in the sample No. 3 is ~62 ± 4%.

CONCLUSIONS

The SEM study of the structural and phase states of the material of the disk blanks of the nickel-based superalloy VV751P subjected to different heat treatment shows the presence of grains of the γ matrix with sizes of 30–50 μm and cuboidal submicroscopic particles of the γ′ phase. The APT study of these materials made it possible to analyze on the atomic scale the distribution of chemical elements in the nanosized particles of the γ and γ′ phases and in the interphase layers. In the studied volumes of the samples of the Ni-based superalloy, only particles of the γ and γ′ phases were found. It was shown that the γ′-phase regions are enriched in Al, Ti, Ni, and Nb (γ′-forming elements), and in the γ phase, the content of Co, Cr, and Mo (γ-forming elements) is enhanced.

The contents of elements such as V, W, Fe, Si, B, and C are relatively close in the γ and γ′ phases, and the character of the enrichment of these phases in these elements depends on the size of the particles. It has been shown that, apart from the usually observed γ′-phase particles in the γ matrix, inside coarse particles of the γ′ phase there are ultra-dispersed regions of the γ phase, or, to be more precise, approximately equiaxed homogeneously distributed clusters of γ-forming elements 1–3 μm in size.

This confirms similar results of foreign APT studies of Ni-based superalloys heavily alloyed with γ-forming elements [8, 9]. Apart from the above-mentioned ultradisperse equiaxed clusters, in this work we found chains of ultradisperse flattened features of approximately the same chemical composition for the first time. For the samples studied, graphs of element concentrations in the particles of the γ and γ′ phases as

functions of the average concentrations of the elements in the alloy have been plotted.

The values of the volume fraction of the γ′ phase in the samples of blanks 1, 2, and 3 estimated based on these graphs were found to be 68 ± 1, 61 ± 2, and 62 ± 4%, respectively. It has been shown that the samples made from blank 1, which is characterized by the largest heat resistance, contain the maximum volume fraction of the γ′ phase. The highest conditional yield stress was found in the samples made of blank 2, where ultra-dispersed precipitates of the γ phase were revealed.

A discussion of the origin of the specific distributions of elements in the γ and γ′ phases, of the possible causes of the formation of ultra-disperse clusters of γ-forming elements and of chains of such clusters, and of the peculiarities of the transition layers between phases is planned to take place in a separate work. The results obtained are important both for a further deepening of the understanding of the physical nature of the NBSAs and for solving practical problems of optimization of the chemical composition and temperature and time conditions of different stages of the technology of production of disks from the NBSAs.

ACKNOWLEDGMENTS

The atom-probe tomographic investigations were performed at the Center of Collaborative Access KAMIKS (http://kamiks.itep.ru/), Kurchatov Institute, National Research Center, Institute of Theoretical and Experimental Physics (ITEF).

REFERENCES

1. H. Fecht and D. Furrer, "Processing of nickel-base superalloys for turbine engine disc applications," Adv. Eng. Mater. **2**, 777–787 (2000).
2. E. N. Kablov, "Innovative developments of FSUE "VIAM" SSC of RF on realization of "Strategic directions of the development of materials and technologies of their processing for the period until 2030," Aviatsionnye Materialy i Tekhnologii, No. 1 (34), 3–33 (2015).
3. G. S. Garibov, "Future development of domestic powdered heat-resistant nickel-based disk alloys for new parts of aviation technology," Tekhn. Legk. Splav., No. 1, 7–28 (2017).
4. A. V. Logunov, *Heat Resistant Nickel Alloys for Gas Turbine Blades and Discs* (Gazoturbinnye Tekhnologii, Rybinsk, 2017).
5. D. V. Zaitsev, S. V. Sbitneva, L. B. Ber, and A. V. Zavodov, "Determination of the chemical composition of the particles of the main phases in products from granulated nickel heat-resistant alloy EP741NP," Trudy VIAM, No. 9 (45), 61–71 (2016).
6. T. Murakumo, T. Kobayashi, Y. Koizumi, and H. Harada, "Creep behavior of Ni-base single-crystal superalloys with various γ′ volume fraction," Acta Mater. **52**, 3737–3744 (2004).
7. A. K. Jena and M. C. Chaturvedi, "The role of alloying elements in the design of nickel-base superalloys," J. Mater. Sci. **19**, 3121–3139 (1984).
8. X. P. Tan, D. Mangelinck, C. Perrin-Pellegrino, L. Rougier, Ch.-A. Gandin, A. Jacot, D. Ponsen, and V. Jaquet, "Atom probe tomography of secondary γ′ precipitation in a single crystal Ni-based superalloy after isothermal aging at 1100°C," J. Alloys Compd. **611**, 389–394 (2014).
9. P. A. J. Bagot, O. B. W. Silk, J. O. Douglas, S. Pedrazzini, D. J. Crudden, T. L. Martin, M. C. Hardy, M. P. Moody, and R. C. Reed, "An Atom Probe Tomography study of site preference and partitioning in a nickel-based superalloy," Acta Mater. **125**, 156–165 (2017).
10. S. V. Rogozhkin, A. A. Aleev, A. A. Lukyanchuk, A. S. Shutov, O. A. Raznitsyn, and S. E. Kirillov, "Atom probe tomography prototype with laser evaporation," Instrum. Exp. Tech. **60**, 428–433 (2017).
11. O. A. Raznitsyn, A. A. Luk'yanchuk, A. S. Shutov, S. V. Rogozhkin, and A. A. Aleev, "Optimization of laser parameters for laser-assisted atom probe tomography characterization," Yadern. Fiz. Inzhinir. **8**, 138–140 (2017).
12. A. A. Aleev, S. V. Rogozhkin, A. A. Luk'yanchuk, A. S. Shutov, O. A. Raznitsyn, A. A. Nikitin, N. A. Iskandarov, O. A. Korchuganova, and S. E. Kirillov, Certificate of state registration of a computer program No. 2018661876 (20 September 2018).
13. O. A. Raznitsyn, A. A. Lukyanchuk, A. S. Shutov, S. V. Rogozhkin, and A. A. Aleev, "Optimization of material analysis conditions for laser-assisted atom probe tomography characterization," J. Anal. Chem. **72**, 1404–1410 (2017).
14. M. K. Miller, *Atom Probe Tomography: Analysis at the Atomic Level* (Kluwer Academic, New York, 2000).
15. L. B. Ber, "Temperature–time diagrams of the decomposition of a γ solid solution in granular heat-resistant nickel alloys EP741NP and VV751P, their construction and use when quenching disk blanks," Tekhn. Legk. Splav., No. 4, 5–19 (2017).